Dynamic Simulation of Droplet Interaction and Self-Assembly in a Nematic Liquid Crystal

Chunfeng Zhou,[†] Pengtao Yue,[†,‡] and James J. Feng*[,†,‡]

Department of Chemical and Biological Engineering, University of British Columbia, Vancouver, BC V6T 1Z3, Canada, and Department of Mathematics University of British Columbia, Vancouver, BC V6T 1Z2, Canada

Received October 23, 2007. In Final Form: December 14, 2007

We use dynamic simulations to explore the pairwise interaction and multiparticle assembly of droplets suspended in a nematic liquid crystal. The computation is based on a regularized Leslie−Ericksen theory that allows orientational defects. The homeotropic anchoring on the drop surface is of sufficient strength as to produce a satellite point defect near the droplet. Based on the position of the defects relative to the host droplet and the far-field molecular orientation, we have identified five types of pairwise attractive and repulsive forces. In particular, long-range attraction between two droplets with their line of centers along the far-field orientation decays as R^{-4}, with R being the center-to-center separation. This agrees with prior static calculations and a phenomenological model that treats the attraction as that between two dipoles. For interaction in shorter ranges, our simulations agree qualitatively with experimental measurements and static calculations. However, there is considerable quantitative discrepancy among the few existing studies and our simulation. We suggest that this is partly due to the dynamic nature of the process, which has never been taken into account in prior calculations. Multidrop simulations show the formation of linear chains through pairwise interactions between nearby droplets. Parallel chains repel or attract each other depending on the relative orientation of the drop-to-defect vector. These are consistent with experimental observations of chain formation and two-dimensional self-assembly in bulk nematics and smectic-C films.

I. Introduction

Common emulsions involve isotropic liquids such as oil and water. When the continuous phase is an anisotropic liquid crystal, the emulsion exhibits unusual microstructures. In their well-known monograph, de Gennes and Prost[1] described the aggregation of bubbles on the free surface of a cholesteric as strings that delineate the molecular orientation. In nematics, Poulin and co-workers carried out a series of experimental observations on pattern formation of suspended particulates.[2−5] Water droplets suspended in the thermotropic liquid crystal pentylcyanobiphenyl (5CB) in the nematic phase form chains with neighboring drops separated by a constant distance, and the chains tend to align with the background nematic orientation.[3] This was later confirmed by experiments using PDMS oil drops in another thermotropic nematic medium.[4,5] The formation of parallel chains requires a strong homeotropic anchoring on the drop surfaces, i.e., with the director $\boldsymbol{n}$ normal to the surface. With planar anchoring or weak homeotropic anchoring, the droplets form kinked lines at an angle with the background orientation.[6−9] Ruhwandl and Terentjev[10,11] obtained analytical solutions in the weak anchoring limit for particles bearing the Saturn ring, and thus provided an explanation for the kinked lines. In the rest of this paper, we limit ourselves to droplets with strong homeotropic anchoring.

Poulin et al.[3,6] proposed a theoretical framework for understanding the self-assembly of droplets into chains. As the water drop possesses homeotropic anchoring on its surface, its inclusion in an otherwise uniformly oriented liquid crystal necessitates the appearance of defects. In this case, a point defect known as a "hyperbolic hedgehog" accompanies each water droplet, and the two form a dipole when viewed from a great distance. Attraction between such dipoles explains the formation of chains of droplets separated by the satellite point defects. Furthermore, the elastic energy incurred by the point defect prevents the neighboring drops from contact and coalescence. Thus, long-range attraction and short-range repulsion both play roles in the formation and stability of the self-assembled pattern. Poulin et al.[3,6] and Lubensky et al.[12] used phenomenological *ansatz* director fields to compute the long-range attraction between neighboring particles as due to the interaction among effective dipoles and quadrupoles.

Qualitatively, the above explanation is clear and convincing. But the nature of pairwise interaction needs to be clarified in a more rigorous way. For example, the dipole−dipole interaction accounts for long-range attractions and predicts $F \sim R^{-4}$ for $R \gg a$, with F being the attraction force, R being the center-to-center separation, and a being the particle radius. Both experimental measurements[13,14] and numerical computations[15]

* Corresponding author. E-mail: jfeng@CHML.UBC.CA.
† Department of Chemical and Biological Engineering.
‡ Department of Mathematics.

(1) de Gennes, P. G.; Prost, J. *The Physics of Liquid Crystals*; Oxford: New York, 1993.
(2) Poulin, P.; Raghunathan, V. A.; Richetti, P.; Roux, D. *J. Phys. II* **1994**, *4*, 1557−1569.
(3) Poulin, P.; Stark, H.; Lubensky, T. C.; Weitz, D. A. *Science* **1997**, *275*, 1770−1773.
(4) Loudet, J. C.; Barois, P.; Poulin, P. *Nature* **2000**, *407*, 611−613.
(5) Loudet, J. C.; Poulin, P.; Barois, P. *Europhys. Lett.* **2001**, *54*, 175−181.
(6) Poulin, P.; Weitz, D. A. *Phys. Rev. E* **1998**, *57*, 626−637.
(7) Mondain-Monval, O.; Dedieu, J. C.; Gulik-Krzywicki, T.; Poulin, P. *Eur. Phy. J. B* **1999**, *12*, 167−170.
(8) Poulin, P.; Francès, N.; Mondain-Monval, O. *Phys. Rev. E* **1999**, *59*, 4384−4387.
(9) Musevic, I.; Skarabot, M.; Tkalec, U.; Ravnik, M.; Zumer, S. *Science* **2006**, *313*, 954−958.
(10) Ruhwandl, R. W.; Terentjev, E. M. *Phys. Rev. E* **1996**, *54*, 5204−5210.
(11) Ruhwandl, R. W.; Terentjev, E. M. *Phys. Rev. E* **1997**, *56*, 5561−5565.
(12) Lubensky, T. C.; Pettey, D.; Currier, N.; Stark, H. *Phys. Rev. E* **1998**, *57*, 610−625.
(13) Poulin, P.; Cabuil, V.; Weitz, D. A. *Phys. Rev. Lett.* **1997**, *79*, 4862−4865.
(14) Noël, C. M.; Bossis, G.; Chaze, A.-M.; Giulieri, F.; Lacis, S. *Phys. Rev. Lett.* **2006**, *96*, 217801.
(15) Fukuda, J.-I.; Stark, H.; Yoneya, M.; Yokoyama, H. *Phys. Rev. E* **2004**, *69*, 041706.

10.1021/la703312f CCC: $40.75
Published on Web 02/20/2008

have borne out this long-range scaling. What becomes of the attractive force as the particles move close to each other? Lubensky et al.[12] used the repulsion between quadrupolar moments to predict a decline of the attraction but could not produce a repulsive force even when $R \rightarrow 2a$. Data of Poulin et al.[13] show that the attraction force F starts to fall below the scaling at $R \approx 3a$. Noël et al.[14] measured F for a wider range of R. The decline of the attraction force for short separations is much steeper than predicted by the model of Lubensky et al. Finally, Fukuda et al.[15] computed the repulsion between two "antiparallel" dipoles, with the two defects on the outer side of the droplets. They found $F \sim r^{-3}$ in the whole range of r from slightly above $2a$ to $9a$, in disagreement with the r^{-4} scaling predicted by dipolar interaction. Thus, there is still much uncertainty about the nature of the pairwise interaction.

More recently, two-dimensional (2D) colloidal crystals have been achieved via nematic-mediated self-assembly.[9,16] They are of potential importance as a novel way to control the stability and structures of colloids[17] and as templates for novel optical materials.[18] In particular, Musevic et al.[9] identified *lateral interaction* between parallel chains as the key mechanism in governing 2D crystallization. As in the study by Poulin et al.,[3] particles with the hedgehog defect form chains along the direction of the background nematic orientation. If another particle is in the vicinity of the chain with its dipole parallel and in the same direction as those in the chain, it is repelled by the chain. Conversely, if the single particle's dipole is opposite to that of the chain (antiparallel configuration), attraction occurs. Hence, antiparallel chains aggregate and form a regular and robust hexagonal lattice. Using an energy minimization procedure similar to that of Fukuda et al.,[15] Musevic et al.[9] computed the equilibrium arrangement of particles, which turns out to be a periodic pattern similar to observations. But the defect separating particles in the chain is a small ring instead of the observed point defect.

All the above computations are concerned with the *static* equilibrium position, which has been sought through a straightforward energy minimization procedure. In reality, the particles move as a result of elastic relaxation, and hence the director field is not at equilibrium until the motion ceases in the end. The process cannot be treated as quasi-static in general, and the *dynamic* pairwise and multiparticle interaction may differ appreciably from predictions based on equilibrium director fields. The dynamic problem is much more difficult than the static one. The motion of the particles is typically driven by an elastic force due to nematic distortion. The fluid flow and evolution of the director field are coupled, and both are in turn dependent on the position and the motion of the particle surfaces on which velocity and anchoring boundary conditions are enforced.

This complex task seems to have been first tackled by Stark and Ventzki[19] using the Leslie−Ericksen theory[1] to model the nematic. Up to now, dynamic simulations have been done on the motion of single particles. Yamamoto[20] developed a scheme for evolving the position of multiple particles by elastic forces in a quasi-static manner. The director field is equilibrated at every step and no fluid motion is involved. But there have been no dynamic simulation on pairwise and multiparticle interactions in the nematic. Previous experiments and computations on a single particle[21−23] have shown rich dynamics in the approach to multiple defect configurations and in the transition among them. For multiple particles, the dynamic evolution will be important to the self-assembly process and therefore warrants an indepth study.

In this paper, we present what appears to be the first dynamical simulation of the self-assembly of multiple droplets in a nematic liquid crystal. The numerical methodology is based on a phase-field representation of the interface and employs finite elements with adaptive meshing to resolve the interfaces as well as defects in the nematic bulk. After describing the numerical methodology and the algorithm, we will report axisymmetric and 2D planar simulations on pairwise interactions and self-assembly of multiple droplets. In particular, we will explore the nature of longitudinal and lateral pairwise interaction forces. In view of prior experimental observations, we will then investigate the formation of chains, chain−chain attraction and repulsion, and 2D assembly of a cluster of droplets. Where possible, comparisons will be made to experiments as well as previous static computations.

II. Theory and Numerical Method

Recently, we have developed a general finite-element algorithm AMPHI for simulating interfacial dynamics in two-component rheologically complex fluids.[24] The interfaces are treated as having a small but finite thickness with a phase-field variable changing continuously from one phase to the other. Fluid properties, such as density and viscosity, and flow quantities, such as pressure and velocity, change steeply yet continuously across the interfaces. Hence, no discontinuity appears in the system. The phase field ϕ, which indicates the position of the interfaces, is governed by a mixing energy consisting of two components, one "hydro"-philic and the other "hydro"-phobic. This energy-based formulation easily incorporates complex rheology as long as the free energies of the microstructures are known. The package has been extensively validated[24] and applied to simulate drop deformation, coalescence, and jet breakup in Newtonian and viscoelastic liquids.[25,26]

The nematic liquid crystal admits a natural energetic description. Bulk distortions may be described by the Frank energy,[1] and surface anchoring can be described by the Rapini−Papoular anchoring energy.[27,28] Thus, the elastic characteristics are easily incorporated into the phase-field framework of AMPHI. Anisotropic viscosities may be introduced via Leslie coefficients. Thus, we have recently adapted AMPHI to explore the defect dynamics around a single drop rising in a nematic phase.[22,29] For the multidroplet simulations to be presented, the code has been generalized to allow periodic boundary conditions in two directions. Details of the theoretical model and computational algorithm can be found in reports by Yue et al.[24,27] and Zhou et al.[22] In the following, we will only summarize the main ideas and give the governing equations.

Consider a two-component immiscible blend of a Newtonian liquid and a nematic liquid crystal. For the problem at hand, we may visualize Newtonian drops of arbitrary shape and size suspended in the nematic medium. The Newtonian bulk is represented by $\phi = -1$ and the nematic by $\phi = 1$, and the interfaces are simply the level set of $\phi = 0$. The governing equations are the continuity and momentum equations supplemented by the Cahn−Hilliard equation for the transport of the phase field ϕ[27] and the Leslie−Ericksen equations for the nematic director $\boldsymbol{n}$:[22]

(16) Nazarenko, V. G.; Nych, A. B.; Lev, B. I. *Phys. Rev. Lett.* **2001**, *87*, 075504.
(17) Loudet, J.; Poulin, P. *J. Dispersion Sci. Technol.* **2002**, *23*, 143−154.
(18) Rudhardt, D.; Fernndez-Nieves, A.; Link, D. R.; Weitz, D. A. *Appl. Phys. Lett.* **2003**, *82*, 2610.
(19) Stark, H.; Ventzki, D. *Europhys. Lett.* **2002**, *57*, 60−66.
(20) Yamamoto, R. *Phys. Rev. Lett.* **2001**, *87*, 075502.
(21) Fukuda, J.-I.; Stark, H.; Yoneya, M.; Yokoyama, H. *J. Phys.: Condens. Matter* **2004**, *16*, S1957−S1968.
(22) Zhou, C.; Yue, P.; Feng, J. J. *J. Fluid Mech.* **2007**, *593*, 385−404.
(23) Khullar, S.; Zhou, C.; Feng, J. J. *Phys. Rev. Lett.* **2007**, *99*, 237802.
(24) Yue, P.; Zhou, C.; Feng, J. J.; Ollivier-Gooch, C. F.; Hu, H. H. *J. Comput. Phys.* **2006**, *219*, 47−67.
(25) Yue, P.; Zhou, C.; Feng, J. J. *Phys. Fluids* **2006**, *18*, 102102.
(26) Zhou, C.; Yue, P.; Feng, J. J. *Phys. Fluids* **2006**, *18*, 092105.
(27) Yue, P.; Feng, J. J.; Liu, C.; Shen, J. *J. Fluid Mech.* **2004**, *515*, 293−317.
(28) Rapini, A.; Papoular, M. *J. Phys. C* **1969**, *30*, 54−56.
(29) Zhou, C.; Yue, P.; Feng, J. J.; Liu, C.; Shen, J. *Phys. Fluids* **2007**, *19*, 041703.

$$\nabla\cdot v = 0 \tag{1}$$

$$\rho\left(\frac{\partial v}{\partial t} + v\cdot\nabla v\right) = -\nabla p + \nabla\cdot\sigma \tag{2}$$

$$\frac{\partial \phi}{\partial t} + v\cdot\nabla\phi = \gamma\lambda\nabla^2\left[-\nabla^2\phi + \frac{\phi(\phi^2-1)}{\epsilon^2}\right] \tag{3}$$

$$h = \gamma_1 N + \gamma_2 D\cdot n \tag{4}$$

where λ, ϵ, and γ are the interfacial energy density, capillary thickness, and mobility of the diffuse interface, respectively. The density $\rho = ((1+\phi)/2)\rho_1 + ((1-\phi)/2)\rho_2$ is an average between the two components. The stress tensor σ in the momentum equation is:

$$\sigma = -\lambda\nabla\phi\nabla\phi - K\frac{1+\phi}{2}\nabla\mathrm{n}\cdot(\nabla\mathrm{n})^T - G + \frac{1+\phi}{2}\sigma' + \frac{1-\phi}{2}\mu[\nabla v + (\nabla v)^T] \tag{5}$$

where G is the anchoring stress of the nematic director on the interface, $G = A(n\cdot\nabla\phi)n\nabla\phi$ for planar anchoring and $G = A[(n\cdot n)\nabla\phi - (n\cdot\nabla\phi)n]\nabla\phi$ for homeotropic anchoring, A is the surface anchoring energy density, K is the bulk elastic constant of the nematics under the one-constant approximation, and μ is the Newtonian viscosity. σ' is the Leslie viscous stress[30,31] in the nematic phase

$$\sigma' = \alpha_1 D{:}nnnn + \alpha_2 nN + \alpha_3 Nn + \alpha_4 \mathrm{D} + \alpha_5 nn\cdot D + \alpha_6 D\cdot nn \tag{6}$$

where α_{1-6} are the Leslie viscous coefficients obeying an Onsager relation $\alpha_2 + \alpha_3 = \alpha_6 - \alpha_5$, so five of them are independent.[1] $D = {}^1/_2[\nabla v + (\nabla v)^T]$ is the strain rate tensor, $\Omega = {}^1/_2[(\nabla v)^T - \nabla v]$ is the vorticity tensor, and $N = (\mathrm{d}n)/(\mathrm{d}t) - \Omega\cdot n$ is the rotation of n with respect to the background flow field. The director field n evolves in the flow field according to a balance between elastic and viscous torques as given in eq 4. The molecular field h, denoting elastic torque in the nematic phase, derives from the free energies of the system:[1]

$$h = K\left[\nabla\cdot\left(\frac{1+\phi}{2}\nabla\mathrm{n}\right) - \frac{1+\phi}{2}\frac{(\mathrm{n}^2-1)\mathrm{n}}{\delta^2}\right] - \mathrm{g} \tag{7}$$

with $g = A(n\cdot\nabla\phi)\nabla\phi$ for planar anchoring and $g = A[((\nabla\phi\cdot\nabla\phi)n - (n\cdot\nabla\phi)\nabla\phi]$ for homeotropic anchoring. The term involving δ arises from regularizing the Frank energy to allow defects:[22]

$$f_{\mathrm{reg}}(n) = K\left[{}^1/_2|\nabla\mathrm{n}|^2 + \frac{(|\mathrm{n}|^2-1)^2}{4\delta^2}\right] \tag{8}$$

Thus, a defect is represented by $|n|$ that falls below unity within a small area of size δ. This regularization is inspired by the Landau−Ginzburg equation[32,33] and amounts to a simplified form of Ericksen's theory with a variable order parameter,[34] with $|n|$ acting as the local order parameter. We have used $\delta = 4\epsilon$ since the defect core size is comparable to the interfacial thickness. Note that in the limit of $\epsilon \to 0$, the diffuse interface model reverts to the classic Navier−Stokes sharp-interface hydrodynamics.[27] In particular, the interfacial tension σ and Rapini−Papoular anchoring constant W can be recovered from the diffuse-interface parameters for small ϵ as $\sigma = 2\sqrt{2}\lambda/3\epsilon$ and $W = 2\sqrt{2}A/3\epsilon$. We have used $\epsilon = 0.01a$ for most of the calculations, a being the radius of the droplets. Previous computations indicate that such an ϵ is small enough to approximate the sharp-interface limit in the present simulations,[24,25] especially because they involve no small-scale phenomenon such as surface rupture.

In axisymmetric and planar 2D geometries, these equations are discretized on a unstructured grid of triangular elements using the Petrov−Galerkin formulation with streamline upwinding for the constitutive equation.[24] A critical ingredient of the algorithm is an adaptive meshing scheme that accurately resolves the drop interfaces as well as the defect cores at a manageable computational cost. As the interface and defects move, the mesh quality is monitored and updated by coarsening and refinement as needed. Time integration is by an implicit second-order scheme with the time step automatically adjusted according to the motion of the interface.[24] Typical grid sizes are $h_1 = 0.006a$ on the interface and near defects, $h_2 = 0.2a$ in the bulk of the drop fluid, and $h_3 = 0.5a$ in the matrix. The meshing module of the program smooths the transition between different regions. Numerical experiments have shown that these grid sizes and the time step used in the simulations are sufficient for numerical convergence.

As a general numerical algorithm for computing nematic-particle interactions, our package is versatile and powerful. We should perhaps mention some of its features, though not all of them will be important to the computations reported below. First, our code accounts for several factors that have been largely ignored in the past. These include the drop deformation, which in some cases may interact with the nematic order in the vicinity of the surface,[29] finite anchoring strength that may conceivably be tuned to manipulate the resultant colloidal structure, and the fully anisotropic rheology of the nematic phase, which plays a major role in the motion of dispersed particulates in a nematic medium.[22] Second, the phase-field formulation has the advantage of simulating topological changes such as interfacial rupture and coalescence naturally under a short-range force resembling the van der Waals force.[35] There is no need for manual intervention as in sharp-interface models to effect such events. Finally, the finite-element method with adaptive meshing makes possible simulations of multiple interfaces and defects in complex geometries while maintaining accurate spatial resolution of the large-gradient regions.

We must note that the code is limited at present to two spatial dimensions. Some of the geometric setups to be simulated are axisymmetric and thus can be readily handled by the code. Others, such as the self-assembly of multiple droplets, occur in 3D, and we are forced to compute a planar 2D analogy of them. However, this is not as severe a restriction as it might appear. Considerable theoretical and experimental work has been done on particle interaction in freely suspended *smectic C films*, where the dynamics is essentially 2D. Such results provide direct benchmarking for our computations. Furthermore, their general similarity to observations in 3D nematics suggests that the underlying physics is common and that our 2D numerical simulations are relevant to 3D reality. More details will be given in the next section.

Some remarks on terminology seem necessary to avoid confusion in discussing the results. The term "2D" has two meanings in this paper. One refers to the 2D patterns formed by particles as opposed to 1D chains. The other refers to the spatial dimensions in the computations. Similarly, we sometime use the term "dipole" to refer to the drop−defect ensemble, with the drop-to-defect vector indicating its orientation. This is to be distinguished from the electrostatic analogy that treats the particle−particle interaction as that between "dipolar" and "quadrupolar" moments.[12] In fact, an important conclusion to be drawn from our simulations is that the pairwise interaction is not of the dipolar nature in general.

III. Results and Discussion

This section has two main parts. The first deals with *pairwise interactions*, with each of the droplets bearing a single hyperbolic hedgehog defect. The two droplets are initially arranged so that their line of centers is parallel or perpendicular to the far-field nematic orientation. These will be called, respectively, the longitudinal and lateral pairs. In each case, the two drop-to-

(30) Leslie, F. M. *Quart. J. Mech. Appl. Math.* **1966**, *19*, 357−370.
(31) Leslie, F. M. *Arch. Rat. Mech. Anal.* **1968**, *28*, 265−283.
(32) Lin, F. H.; Liu, C. *Arch. Rat. Mech. Anal.* **2000**, *154*, 135−156.
(33) Liu, C.; Walkington, N. J. *SIAM J. Numer. Anal.* **2000**, *37*, 725−741.
(34) Ericksen, J. L. *Arch. Rat. Mech. Anal.* **1991**, *113*, 97−120.
(35) Yue, P.; Feng, J. J.; Liu, C.; Shen, J. *J. Colloid Interface Sci.* **2005**, *290*, 281−288.

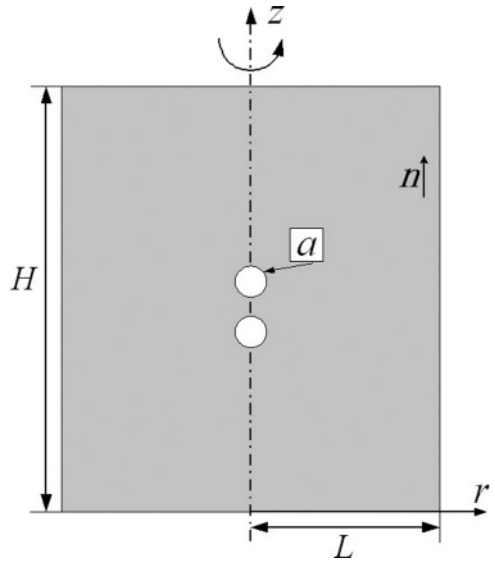

Figure 1. The geometry of the computational domain. The radius of the drops is *a*. With axisymmetry around the *z* axis, the domain is half of the meridian plane. For 2D computations, the domain is the entire rectangular box.

defect dipoles may be in the same direction (parallel) or opposite to each other (antiparallel). Special attention will be given to the pairwise interaction forces in connection with the open questions in the literature regarding the dipolar nature of this interaction. The second part explores the interaction and self-assembly of *multiple droplets*. We will study the formation of linear chains, interaction between neighboring chains in parallel and antiparallel orientations, and finally 2D assembly of droplets in a doubly periodic domain.

For a longitudinal pair of droplets, the geometry is axisymmetric. For the other configurations, the real physics is 3D and we are forced to simulate a 2D analogue of it in a planar domain. With axisymmetry, the computational domain is half of the meridian plane, as shown in Figure 1. The rectangular domain has a width of $L = 15a$ in the radial direction and length $H = 24a$ along the axis of symmetry, where a is the drop radius. The two droplets are located on the z axis with top−bottom symmetry at some initial separation. The outer boundary at $r = L$ is a nonslip wall, and periodic boundary conditions are imposed on the top and bottom. The z axis has symmetric boundary conditions for all the variables, $\partial/\partial r = 0$. Note that no boundary conditions are needed on the drop surfaces; velocity and shear-stress continuities occur naturally, and the interfacial tension is accounted for by the interfacial stress $-\lambda\nabla\phi\nabla\phi$ in eq 5. The 2D domains are rectangles with periodic conditions in the vertical or both directions. For the former, the nonperiodic boundaries are nonslip walls with rigid anchoring.

The initial $n(r)$ field is uniformly vertical everywhere except within a small distance from each drop; in this shell n aligns radially. Thus, the initial director field has an abrupt jump between the near-field and far-field orientation. After the simulation starts, there is a rapid rearrangement in the near field, resulting in a point defect near each droplet. For all cases except one (cf. Figure 4), this initial transient is short and insignificant to the ensuing dynamic evolution of the director field. Even though the director does not distinguish between n and $-n$ in reality, we have found the direction of n a convenient means to control the location of the defect. If the far field n is upward and the near field is radially outward, the point defect will nucleate below the drop. Changing either will put the defect above the drop. This scheme will be used to produce parallel and antiparallel dipoles in the simulations.

The complete set of dimensionless groups governing our system is

$$\alpha = \frac{\rho_2}{\rho_1}\ (\text{drop-to-matrix density ratio}) \tag{9}$$

$$\beta = \frac{\mu}{\alpha_4/2}\ (\text{drop-to-matrix viscosity ratio}) \tag{10}$$

$$A_K = \frac{Wa}{K}\ (\text{anchoring-to-bulk energy ratio}) \tag{11}$$

$$A_\sigma = \frac{W}{\sigma}\ (\text{anchoring-to-interfacial tension ratio}) \tag{12}$$

$$Re = \frac{\rho_1 Ua}{\eta}\ (\text{Reynolds number}) \tag{13}$$

$$Ca = \frac{\eta U}{\sigma}\ (\text{capillary number}) \tag{14}$$

along with the various length ratios of the geometry and the ratios between the Leslie viscous coefficients. *Re* and *Ca* are defined using a characteristic velocity $U = K/(\eta a)$ and the viscosity $\eta = (\alpha_3 + \alpha_4 + \alpha_5)/2$ that is the average between the largest and smallest Miesowicz viscosities.[1] The ratio α_3/α_2 distinguishes "flow-aligning" nematics from "tumbling" ones in simple shear flows. In the complex flows due to droplet self-assembly, this distinction is insignificant. Experiments have also used a wide range of thermotropic and lyotropic liquid crystals of both aligning and tumbling types. We have adopted the Leslie viscosities of a common nematic MBBA at 25 °C for all computations:[1] $\alpha_1 = 6.5$, $\alpha_2 = -77.5$, $\alpha_3 = -1.2$, $\alpha_4 = 83.2$, $\alpha_5 = 46.3$, and $\alpha_6 = -32.4$ centipoise (cP). Furthermore, we have assumed that the isotropic drop phase has the same density as the nematic medium and the same viscosity as the isotropic part of the nematic viscosity; $\alpha = 1$, $\beta = 1$. For the anchoring energy W, prior experiments cited "strong anchoring" without giving a value[6] while computations typically assumed rigid anchoring.[12] In all the computations, we have used a large $A_K = 100$. In addition, W is typically much smaller than the interfacial tension σ.[36] We have used $A_\sigma = 0.2$. This, along with a small $Ca = O(10^{-3})$, ensures that the droplets never deviate visibly from the spherical shape. The Reynolds number $Re = O(10^{-2})$ for all the computations and inertia is negligible.

In presenting the results, we have used two different methods to visualize the nematic orientation (Figure 2). The first is a computed light intensity map through crossed polarizers, which would correspond to birefringent images recorded in the experiments. This will be used for the longitudinal pairs in axisymmetric geometry. The numerical scheme is detailed by Han and Rey.[37] For a satellite point defect near a drop, Figure 2a shows the light intensity map along with vector lines for the director field $n(r)$. The pattern of two bright lobes separated by a darker line, with the point defect at the tip, closely resembles experimental pictures in the literature.[13,14,23] The second presentation (Figure 2b) uses contours of $(n_x^2 - 1/2)^2$ in a 2D planar domain, where n_x is the horizontal component of n.[20,38] Thus, bright areas indicate a horizontal or vertical n, while dark areas have n at a 45° angle. The point defect is clearly marked by the

(36) Sonin, A. A. *The Surface Physics of Liquid Crystals*, 1st ed.; Gordon and Breach Publishers: 1995.
(37) Han, W. H.; Rey, A. D. *Macromolecules* **1995**, *28*, 8401−8405.
(38) Yamamoto, R.; Nakayama, Y.; Kim, K. *J. Phys.: Condens. Matter* **2004**, *16*, S1945−S1955.

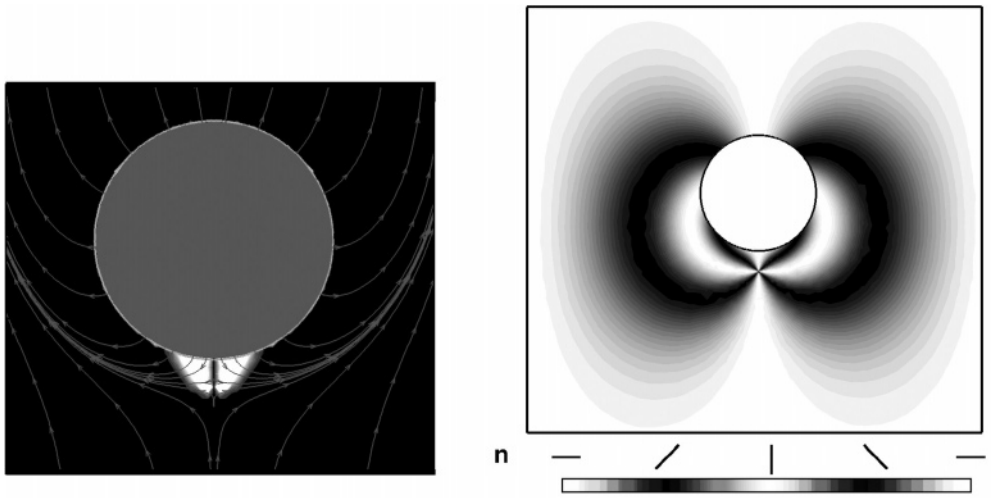

Figure 2. Representation of the director field: (a) birefringent pattern for an axisymmetric *n* field through crossed polarizers; (b) grayscale representation of *n* in 2D geometries with contours of $(n_x^2 - 1/2)^2$. White indicates a vertical or horizontal *n*, while black means a 45° tilt.

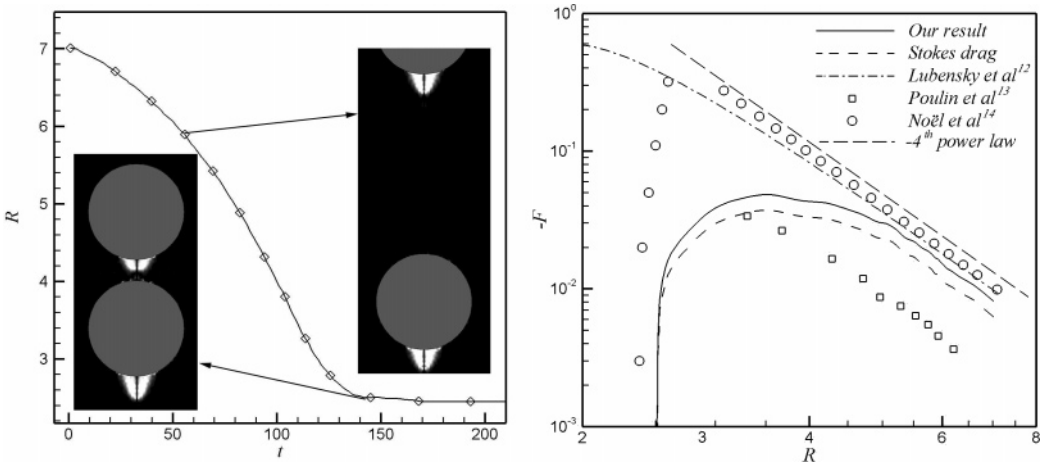

Figure 3. Attraction between a longitudinal pair of drops in the parallel configuration. Time is made dimensionless by the elastic relaxation time $\tau_e = \eta a^2/K$, length is made dimensionless by a, and force is made dimensionless by $4\pi K$. The same nondimensionalization is used for all later plots. (a) The center-to-center distance R as a function of time. The insets show the defect configuration, visualized as in Figure 2a, at time $t = 56.1$ and 145.1. (b) The attraction force $F(R)$, computed by integrating the elastic stress around the drop, compared with prior experimental data (symbols) and theoretical results (lines). The dash line is the drag force estimated from eq 16, and the dash-dot line is the phenomenological F_P of eq 15. The long-dash line indicates the R^{-4} scaling.

focal point from which four dark brushes emanate. The gradient of the grayscale indicates the degree of elastic distortion, which reaches a maximum at the point defect and dies off in the far field.

A. Pairwise Interactions. 1. Longitudinal Pairs. Consider first the interaction of two particles in the parallel configuration, with a center-to-center distance of R. The defects are on the line of centers, which is parallel to the far-field director orientation. Representing the long-range force by the interaction of dipolar and quadrupolar moments, Lubensky et al.[12] constructed a phenomenological formula for the attraction force F_P between the particles:

$$\frac{F_P}{4\pi K} = -24.97\left(\frac{a}{R}\right)^4 + 62.21\left(\frac{a}{R}\right)^6 \qquad (15)$$

Note that the dipolar attraction (the first term) dominates the quadrapolar repulsion (the second term) at large distances. Mathematically, the repulsive force becomes significant for smaller R, but the formula is supposed to be used only for $R \gg a$. In the rest of the paper, we will use the same sign convention, i.e., repulsion being positive and attraction being negative.

In our dynamic simulation in the axisymmetric computational domain of Figure 1, the two droplets indeed attract each other, and their separation decreases in time from an initial $7a$ to a final equilibrium value $R_e = 2.45a$ (Figure 3a). The speed of approach increases initially as R shrinks and reaches a maximum around $R = 3.5a$. Afterward, the speed quickly drops to zero. In the equilibrium state, one point defect is roughly midway between the two drops, a distance of $1.22a$ from either drop center. Compared with the position of the point defect near a single drop,[22] the defect between the droplets is "compressed". The other defect is at a greater distance of $1.32a$, which is close to that of a single drop. Note that the equilibrium separation of $2.45a$ agrees with prior experimental[14] and numerical results[21] to within 3%. The $R(t)$ curve closely resembles that of Poulin et al.[13] In the experiment, the particles' approach takes about 5 s, which corresponds to a dimensionless time of 136 and is comparable to that in Figure 3a.

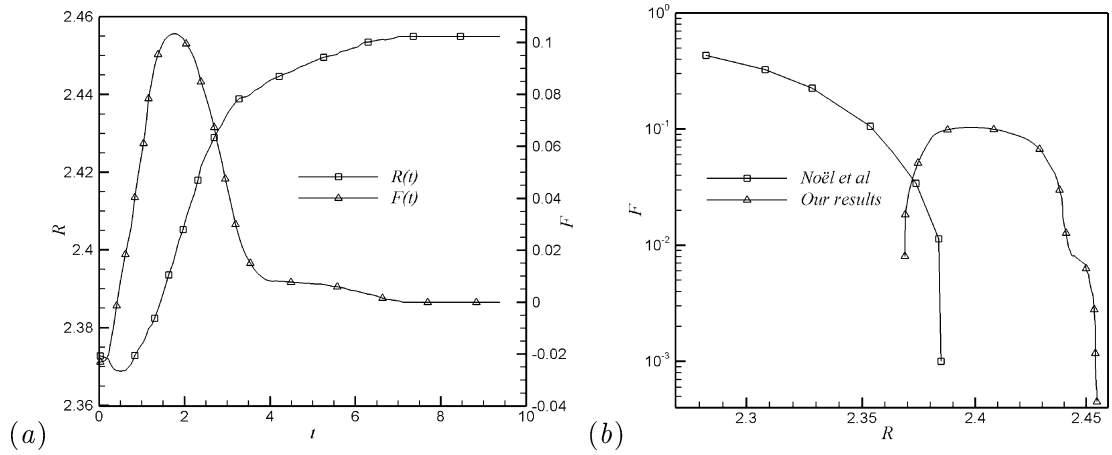

Figure 4. Interaction between a parallel longitudinal pair of droplets with an initial separation smaller than the equilibrium value. (a) Temporal evolution of the center-to-center distance $R(t)$ and elastic force $F(t)$. F is computed by integrating the elastic stress, and positive values denote repulsion. (b) Comparison between the computed $F(R)$ and the ones measured by Noël et al.[14]

We have also computed the instantaneous attractive force F between the droplets, by integrating the *elastic stress components* over the drop surface, and this is plotted in Figure 3b. To extract an attractive force from the particle trajectory, Poulin et al.[13] calculated a Stokes drag with an "effective viscosity" μ_e measured from a capillary tube:

$$F_D = 6\pi\mu_e aV \tag{16}$$

where V is the instantaneous velocity of the particles. Then F is equated to F_D by assuming zero inertia for the particles. In our computations, $Re \sim 10^{-2}$ and inertia is negligible. But strictly speaking, the idea of a constant effective viscosity is suspect since the anisotropic viscosity may vary significantly depending on the flow field.[22] As a test of eq 16, we have computed F_D by taking μ_e to be η, the average between the largest and the smallest of the Miesowicz viscosities. This turns out to be a reasonable approximation of F; it is about 12% smaller in magnitude but follows the same trend. The discrepancy comes from the choice of μ_e. Since the nematic director is mostly normal to the drop surface, it is no surprise that μ_e underestimates the local viscosity and hence the drag force F_D.

For large separations ($R > 5a$), all computations and measurements agree with the fact that the attraction force F obeys the R^{-4} scaling. This is consistent with the dipolar attraction in eq 15. The magnitude of our F is slightly below Lubensky et al.'s formula and Noël et al.'s data. Poulin et al.'s data, however, are lower by a factor of about 4. This may be due to their using a μ_e in eq 16 that is too low. Prior studies[13,14,21] put the lower bound of R for the R^{-4} scaling between $3a$ and $4a$, whereas our F starts to fall below the power law at $R \approx 5a$. The reason for this difference is unclear at present. Our F reaches a maximum near $R = 3.6a$ and then declines with decreasing R. The data of Noël et al. show a much stronger attraction for smaller R followed by a precipitous drop within $R \approx 2.5a$. Thus, their interaction is much more "hard-sphere-like", with a shorter range than in our case. Equation 15 is a poor approximation for short-range interaction, as expected. The quadrupolar repulsion is far too weak to represent the decline of attractive force with decreasing R. In fact, the formula never predicts much reduction in the attraction before the drops touch.

If the drops are initially closer than the equilibrium separation R_e, they are expected to repel each other. To explore this scenario, we simulated the separation of two droplets from an initial separation of $2.37a$. Upon start of the simulation, the $\boldsymbol{n}$ field relaxes into one with two point defects, similar to the insets of Figure 3a. This elastic relaxation, an artifact due to the initial condition, produces the anomalous behavior in Figure 4 for the initial period of the simulation ($t \lesssim 2$). At the beginning, R decreases momentarily ($t \lesssim 0.5$) before increasing with time. Then the droplets separate from each other with increasing velocity until $t \approx 2$. With negligible inertia, the acceleration reflects the changing forces on the droplets. Indeed, the repulsive force F also increases with R in this period, which is counterintuitive. Since time t is scaled by the elastic relaxation time $\tau_e = \eta a^2/K$, the duration of this initial transient ($t \approx 2$) being of order one is reasonable. Only afterward does F decrease with increasing R as expected. The motion ceases at an equilibrium separation of $R_e = 2.45a$, the same value as that reached in the pairwise attraction simulation of Figure 3. Therefore, only the latter part of the simulation, with $t > 2$ and $R > 2.4$, can be meaningfully compared with static measurements of $F(R)$ (Figure 4b). The numerical result parallels the trend of the experimental data,[14] although is shifted to larger R, again indicating longer range interaction in our computation than in the experiment. Incidentally, Noël et al.[14] reported that pushing the two particles too close will result in the point defect opening into a ring. Our simulations show the same transition for initial separations below $2.37a$.

We turn our attention now to two droplets in the antiparallel configuration with the two point defects lying outside of the pair, one on the top of the upper drop and the other below the lower drop. The initial center-to-center separation between the drops is $2.5a$. There is a rapid elastic relaxation at the beginning of the run, but unlike in Figure 4, this transient is insignificant compared with the length of the simulation. The two droplets separate in time with a slowly decreasing velocity (Figure 5a). The simulation is terminated as R reaches $10a$, and the droplets get close to the top and bottom of the computational domain (cf. Figure 1). At that time, the two are still moving apart very slowly. As before, we plot the repulsion force F as a function of R in Figure 4b. For R value up to $6a$, F decays as $R^{-1/3}$. For larger separations, the decline of F becomes even milder.

Fukuda et al.[21] computed the static repulsion between two antiparallel dipoles fixed in space. Their results show the scaling $F \sim R^{-3}$, which is in disagreement with the R^{-4} scaling expected, at least for large R, from dipolar interactions. Why does our F exhibit an even slower decay? For the last part of the simulation, say $R > 6a$, one can imagine that the periodic boundary conditions on the top and bottom of the domain have introduced an

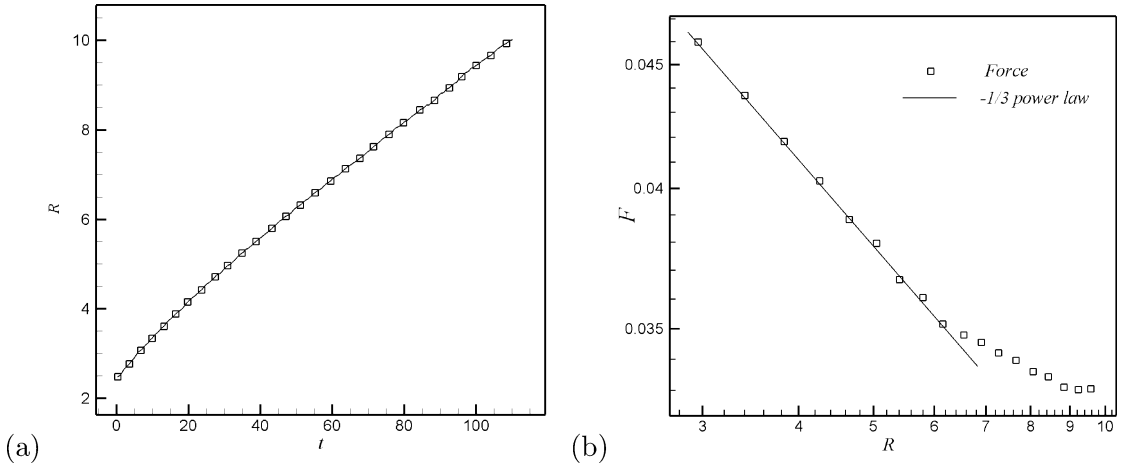

Figure 5. The repulsion between an antiparallel longitudinal pair. (a) The separation $R(t)$ increases from an initial value of $2.5a$. (b) The repulsion force F has a long range and decays slowly with R.

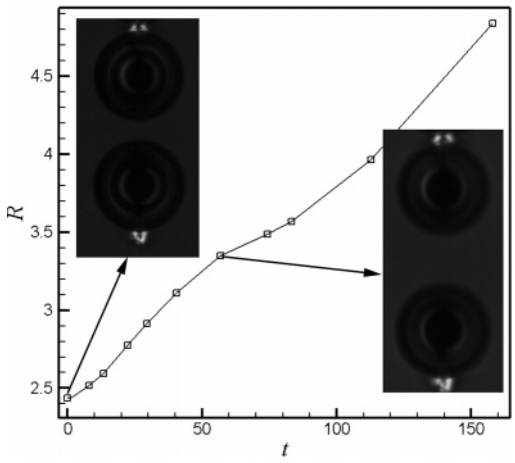

Figure 6. Experimental observation of the repulsion between an antiparallel pair of droplets. The insets are images through crossed polarizers. The drop on top is at the end of a vertical chain (not shown) with upward dipolar orientation. R and t are made dimensionless by the drop radius a and $\tau_e = \eta a^2/K$, with $\eta = 0.0765$ Pa·s, $a = 50\ \mu$, and $K = 10^{-11}$ N.

interference. A plausible explanation for the mild $R^{-1/3}$ initial decay is the dynamic nature of our simulation. As the droplets move apart, the surrounding director field is continuously evolving. This will produce a different elastic force on the droplets than when the droplets are fixed in space. Even though the total simulation lasts more than $100\tau_e$, the drops move an appreciable $0.1a$ apart within τ_e. Therefore, the velocity of separation is too high for the process to be considered quasi-static.

To probe the antiparallel repulsion further, we have conducted an experiment on the interaction among droplets of silicone oil in the nematic 5CB. Occasionally the antiparallel configuration appears and repulsion is observed. We present one such scenario in Figure 6, where a single droplet (at bottom) is repelled by another (at top) with an opposite dipolar direction, the latter being the end of a chain of particles with upward dipoles. Over the entire period of observation, the separation R increases almost linearly in time. If we ignore the later portion of the data (say $R > 3.5a$) because nearby droplets may have interfered, there does appear to be a weak power-law decay of the velocity $v \sim R^{-0.5}$ for the range of $2.6a < R < 3.5a$. This implies that the repulsion force also decays weakly according to $F \sim R^{-0.5}$. That this power law is much closer to our dynamic computation than prior static computations lends support to our argument above.

2. Lateral Pairs. When a pair of droplets are placed side by side, with their line-of-centers orthogonal to the far-field nematic orientation, the geometry is no longer axisymmetric. Therefore, we resort to 2D planar simulations for lateral pairwise interactions. The same is true for the multiple particle interactions in the next section. Fortunately, 2D dynamics can be realized experimentally by incorporating relatively large particles or droplets into freely suspended smectic-C and smectic-C* films.[39] In fact, considerable research has been devoted to this special setup as a rare opportunity to study "anisotropic, two-dimensional emulsions".[40] The 2D character greatly simplifies theoretical analysis[41,42] and facilitates experimental observations.[43] For example, in a smectic-C* film of thickness smaller than the helical pitch, the droplets are observed to interact through the accompanying point defect and form chains, in qualitatively the same fashion as in 3D nematics.[39] Therefore, our 2D simulations enjoy greater relevance to reality than can be generally expected.

Consider first, the parallel configuration for a lateral pair with their dipole direction initially in parallel (Figure 7). The rectangular computational domain has a horizontal width of $17a$ and a height of $10a$, and the two drops are initially placed side by side in the middle with a separation of $3.33a$. Upon start of the simulation, there is again a very brief transient caused by the initial $\boldsymbol{n}(\boldsymbol{r})$ field relaxing to lower the elastic distortional energy. As the two hedgehog defects take shape, they move inward toward each other. There is no rotation of the drops in this process. Then the two droplets repel each other and move apart laterally (Figure 7a). This motion slows down in time and eventually stops at a dimensionless time $t \approx 80$. The apparent steady-state has a drop separation $R_e = 4.02a$ and an angle between the two dipoles of 46.9°.

Musevic et al.[9] measured the interaction potential for a single particle when it is placed beside a chain of particles in 5CB, with the dipole of the single particle parallel to that of the chain. Although their result may have involved contributions from multiple particles in the chain, we have estimated their repulsion force F and compared it with our numerical result in Figure 7b. Two differences stand out. Our F is several times smaller, and it drops to zero rather abruptly at a relatively short separation. The larger F in Musevic et al.'s measurement is probably due

(39) Cluzeau, P.; Poulin, P.; Joly, G.; Nguyen, H. T. *Phys. Rev. E* **2001**, *63*, 031702.
(40) Völtz, C.; Stannarius, R. *Phys. Rev. E* **2004**, *70*, 061702.
(41) Pettey, D.; Lubensky, T. C.; Link, D. R. *Liq. Cryst.* **1998**, *25*, 579−587.
(42) Cluzeau, P.; Bougrioua, F.; Joly, G.; Lejcek, L.; Nguyen, H. T. *Liq. Cryst.* **2004**, *31*, 719−726.
(43) Dolganov, P. V.; Demikhov, E. I.; Dolganov, V. K.; Bolotin, B. M.; Krohn, K. *Eur. Phys. J. E* **2003**, *12*, 593−597.

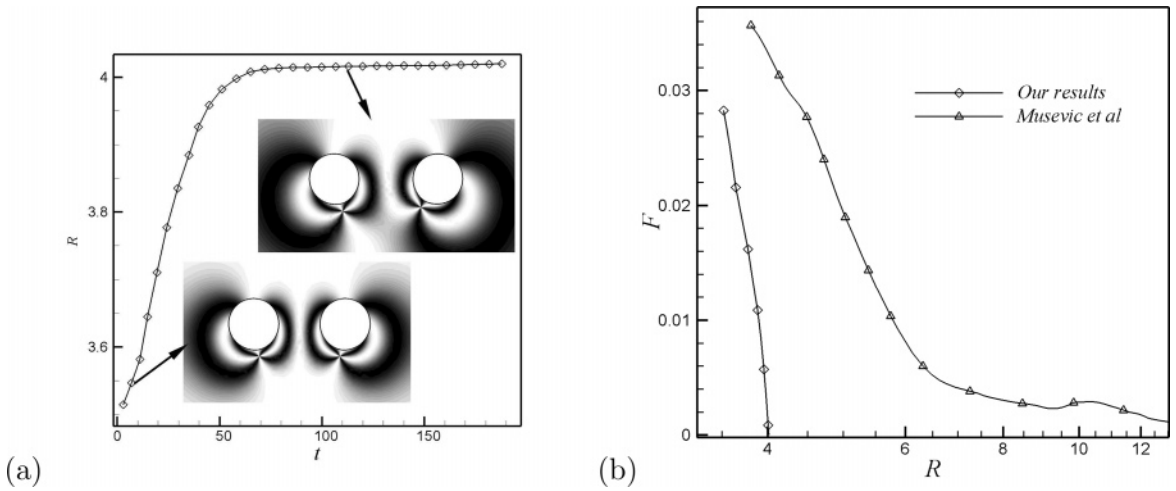

Figure 7. The interaction between a lateral pair of droplets in the parallel arrangement. (a) The center-to-center distance $R(t)$ increases as the droplets repel each other. The n field is visualized as in Figure 2b in the insets. (b) The repulsion force F as a function of R in the dynamic simulation. The data of Musevic et al.[9] are also shown for comparison.

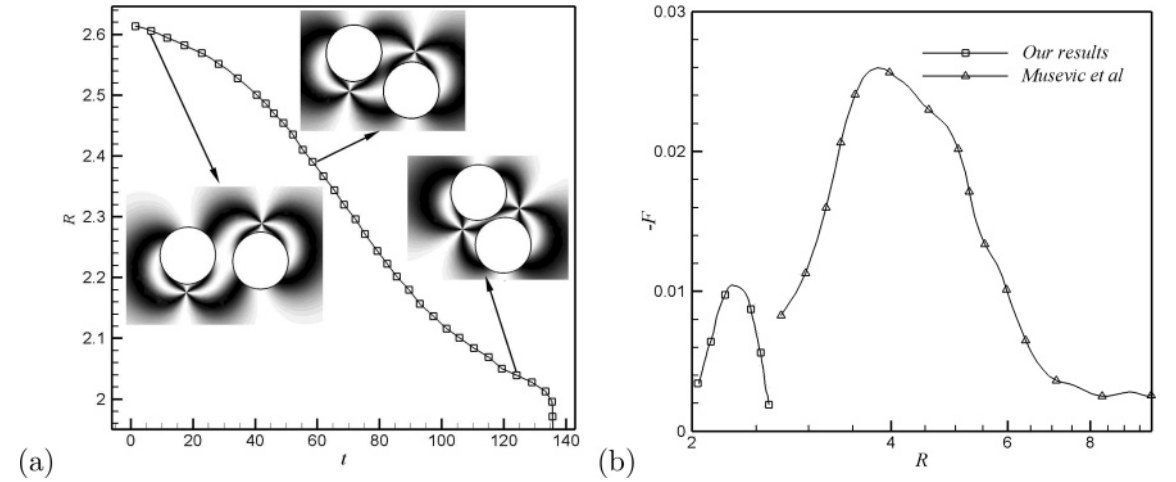

Figure 8. The interaction between a lateral pair of droplets in the antiparallel arrangement. (a) The center-to-center distance $R(t)$ decreases as the drops approach each other. Their line of centers also rotates clockwise. In the end, the two droplets coalesce. (b) The attractive force F as a function of R in the dynamic simulation. The data of Musevic et al.[9] are also shown for comparison.

to repulsion from neighboring particles in the chain. The short range of our F may have to do with the side walls on which fixed vertical anchoring is imposed. Besides, the drop-to-defect vectors tilt toward each other as the drops separate. This configuration promotes attraction between drops (cf. Figure 10), which may have shortened the range of repulsion relative to that for parallel dipoles. Note also that the simulation is dynamic in a 2D geometry, while the experiment is static in 3D next to a substrate. It is difficult to speculate on the implications of such factors for F.

Additional measurements of Musevic et al.[9] suggested that a lateral pair with their dipoles in antiparallel arrangement will attract each other. We have simulated such a scenario in the same computational domain as above, with the droplets initially side by side at a separation of $2.62a$ (Figure 8). The droplets not only approach each other laterally but also shift vertically so as to move the two point defects closer (see insets). As the line of centers makes an angle of roughly 23° with the vertical far-field nematic orientation ($t = 125$), the two point defects sit on opposite sides of the line of centers instead of moving into the gap between the droplets. Soon afterward, the two drops coalesce at $t = 136$. In this process, the attractive force F varies nonmonotonically with the separation R, with a peak at $R = 2.3a$ (Figure 8b). With decreasing R, the attraction initially increases as one would expect. Then the relative rotation between the droplets changes the defect configuration and the nature of the attraction. This causes the decline of the attraction force for $R < 2.3a$.

In the static measurements of Musevic et al.,[9] a single particle is placed beside a chain of particles, with its dipole antiparallel to that of the chain. The single particle is not abreast with one in the chain but rather is staggered between two neighboring ones (cf. Figure 11a). Thus, the measured F comes from two or more particles in the chain, and there is no relative rotation among the particles as exhibited by our doublet. Subject to these complications, perhaps only the initial portion of our result, say $R > 2.4$ in Figure 8b, is comparable with the experimental data. Similar to the repulsion between a parallel pair (Figure 7b), our force is smaller in magnitude and also occurs in a much shorter range than in the experiment. The apparent agreement in the humped shape of the curves is probably fortuitous. In the experiment, the attraction dies down when the single particle is pushed too close to the chain. In our simulation, on the other hand, the two drops maneuver in two dimensions. The downturn in the attraction force with shrinking R is due to the evolving defect pattern toward the end.

To summarize the results and discussion in this subsection, our simulations reproduce the characteristics of pairwise interactions as measured in experiments and predicted by ad hoc models. For longitudinal doublets, a parallel pair tends to attract each

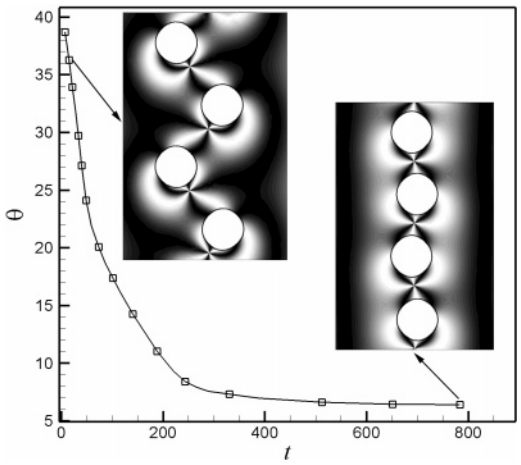

Figure 9. Four droplets assemble into a vertical chain in a vertically aligned nematic phase. The height of the domain is 12.5*a*, with periodic conditions in the vertical direction. The side walls are 20*a* apart and are not shown in the plots. The angle θ, between the neighboring drops and the vertical axis, decreases from 39° toward zero.

other while an antiparallel pair repels, unless their initial separation is very small. For lateral pairs, parallel pairs repel while antiparallel ones attract. Besides, computations and measurements exhibit common trends in the magnitude of the forces. For example, longitudinal interactions are stronger than lateral ones. For longitudinal pairs, the parallel attraction is greater than the antiparallel repulsion, whereas for lateral pairs, the parallel repulsion and the antiparallel attraction have comparable magnitudes. These can be rationalized by the relative position of the point defects, as it determines the elastic distortion surrounding the droplets.

Quantitatively, the long-range longitudinal attraction between parallel pairs is the only situation with a well-established scaling ($F \sim R^{-4}$), which is consistent with the simple picture of dipole−dipole attraction. For closer ranges, the inter-particle force shows considerable divergence among different computational and experimental studies. To a large extent, this discrepancy reflects the dynamic nature of the interaction when the particles are allowed to move. However, a clearer understanding requires more careful computations as well as measurements that account for complicating factors such as differences in spatial dimensionality and the presence of substrates.

B. Multidrop Interactions. 1. Chain Formation. Among experimental observations, the most prominent feature of self-assembly is the formation of chains parallel to the far-field director orientation.[6] We simulate this by arranging four droplets in a regular zigzag pattern in a rectangular domain (Figure 9 inset), with initial center-to-center separation of 3*a* and the line of centers making an angle of 39° with the vertical. The width of the domain is 20*a*, and its height is 12.5*a*. The director is fixed in the vertical direction on the side walls, where the velocity vanishes. Periodic boundary conditions are used for the upper and lower boundary. As before, the initial director field has a thin ribbon of radially outward orientation around each drop, outside of which ***n*** points uniformly upward.

Upon start of the simulation, the director field near each droplet quickly rearranges itself and produces a satellite point defect. These defects are not directly above or below the drop, as one would expect for a single droplet in an otherwise vertically oriented nematic phase. Rather, the droplet−defect dipole points toward the neighboring drop below it (Figure 9). Then, each drop experiences attraction from both neighbors, according to the pairwise attraction force of Figure 3. The net effect is to pull the drops into a straight line. Since this horizontal force is proportional to sin θ, where θ is the angle between the line-of-centers and the vertical, the motion is fast initially when θ is large and slows down toward the end as $\theta \rightarrow 0$.

The process of chain formation is qualitatively the same as observed in 3D nematics[3,6] and 2D smectic C* films.[39] However, the periodicity of the computational domain in the vertical direction introduces an artifact. As the four-particle array is repeated above and below, the equlibrium interparticle separation R_e is predetermined as $^1/_4$ of the height of the domain, independent of the physical parameters of the system. In this case, $R_e = 3.125a$ is somewhat higher than the 2D observation of $2.6a$.[39] Note also that we have used the regular zigzag initial configuration for ease of analyzing the forces in the droplets. Similar chains should form from a more random initial configuration. We will explore such a scenario toward the end.

2. Chain−Chain Interactions. Experiments indicate that chain−chain interaction is central to the formation of regular 2D arrays.[9] From a fundamental viewpoint, chain−chain interaction is more complex than pairwise interactions since it involves the collective motion of multiple particles and defects. Motivated by the experiment of Musevic et al.,[9] we have simulated the interaction between two chains, each consisting of four droplets, in the parallel and the antiparallel configurations.

The computation domain has a width of 18*a* and a height of 13.3*a*, and the boundary conditions are the same as in Figure 9. The parallel chains are initially separated by a center-to-center distance of $R = 3.2a$ (Figure 10a). The defects are directly below the droplet and the chains are parallel to the far-field director orientation. Upon start of the simulation, the two defects at the bottom of the chains quickly move inward toward each other (Figure 10a). This is reminiscent of the defect motion in the lateral pair of Figure 7. Meanwhile, the other three pairs of defects are confined between the neighboring droplets and are not free to move. In view of the pairwise repulsion, one expects the two chains to move laterally away from each other in time. This is largely true, except for the two droplets at the bottom. By breaking the mirror symmetry, the left droplet moves downward while the right one moves upward, with the two forming an attractive doublet similar to that in Figure 3. At this point, the motion of the droplets has practically stopped, and a steady-state configuration emerges. The symmetry breaking may have been triggered by numerical noise such as asymmetry in the unstructured grid but is indicative of the instability of the symmetry pattern. The branched conformation closely resembles experimentally observed patterns for water droplets in a 3D nematic phase, e.g., Figure 11 of Poulin and Weitz.[6]

We have also computed the repulsive force F on one of the upper particles and plotted $F(R)$ in Figure 10b. Based on the pairwise repulsion shown in Figure 7, we expect F to decline monotonically with R. The curious rise for $3.2a < R < 3.5a$ is not due to the initial elastic relaxation, since its duration is roughly 20 times the elastic timescale τ_e. Rather, it is the result of the complex dynamic interaction between the chains. As the two bottom drops attract each other, their attraction force "propagates" up the chains as if along a string. This amounts to an additional attraction on the upper drops, which weakens the repulsion force for the initial period. As the two bottom particles approach, their attraction dies out and so does this effect. Then the repulsion force F assumes its normal decay with R. The magnitude of F is between that of our pairwise repulsion and Musevic et al.'s measurement in Figure 7. Therefore, interaction with multiple particles is responsible, partly at least, for the larger repulsion force here and in Musevic et al.'s experiment than our pairwise

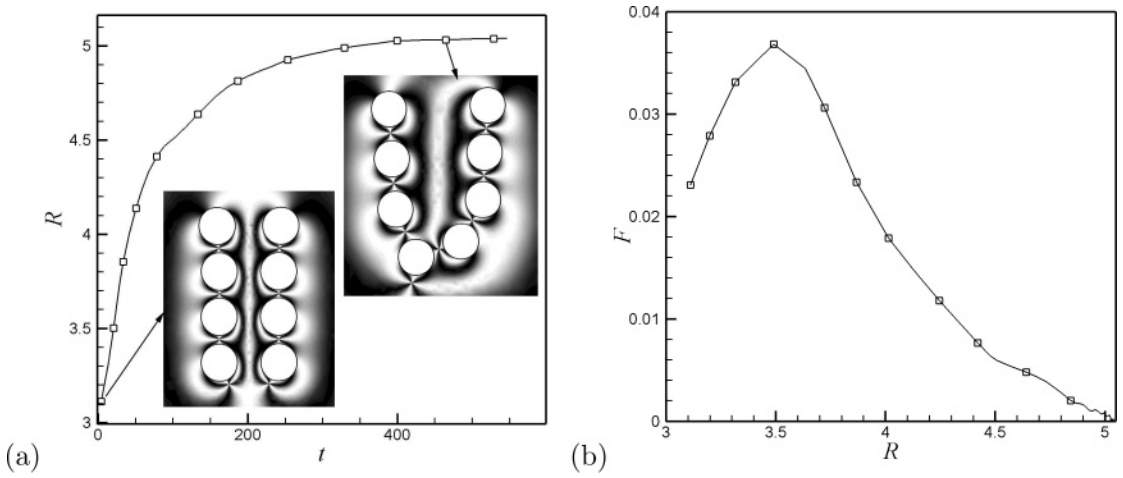

Figure 10. Interaction between two chains in the parallel arrangement. (a) Separation between the second drops from the top. (b) Repulsion force on the second drop from the top of the right chain.

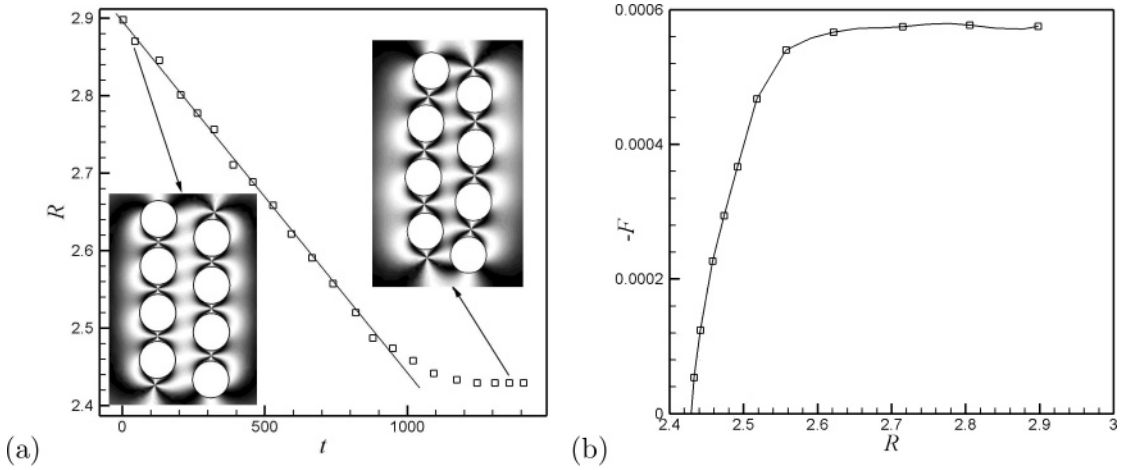

Figure 11. Interaction between two chains of droplets in the antiparallel arrangement. (a) The separation between the chains $R(t)$ decreases from an initial value of $2.9a$ to an equilibrium one of $2.44a$. (b) The attractive force F, averaged among the droplets, as a function of R in the dynamic simulation.

repulsion. Note also that F decays over a longer range than the pairwise repulsion, and the steady separation is larger. These are consistent with the idea that for the pairwise interaction in Figure 7, the tilting of the drop−defect vectors toward each other promotes attraction and suppresses repulsion.

The attraction between antiparallel chains turns out to be simpler as it does not greatly distort the conformation of each chain (Figure 11). The initial condition is similar to that of Figure 10a, but the right chain is flipped vertically so that the point defect is on top of each droplet. The two chains are also offset vertically by a distance of a. The initial separation between the lines of centers is $2.9a$. This setup approximates to what Musevic et al.[9] used experimentally. The two chains approach each other with a velocity that is roughly constant up to $t = 900$. Afterward, the motion slows down, and at $t \approx 1300$, the chains approach an equilibrium state with a separation of $2.44a$ between the centerlines (Figure 11a). This is reasonably close to the experimental value of $2.31a$.[9]

The chain−chain attraction F, plotted in Figure 11b, differs markedly from the pairwise attraction in Figure 8b. First, $F(R)$ does not show the humped shape. The decline with shrinking R should be compared with a similar decline in Musevic et al.'s data[9] in Figure 8b rather than our computed pairwise attraction, as the latter is due to the rotation of the doublet that is absent here. Perhaps because our initial separation is too small, F in Figure 11b does not exhibit the experimentally recorded long-range regime, where the attraction decays with the chain−chain separation. Starting from an initial separation of $4a$, the chains barely move in thousands of time units, indicating $F \approx 0$ for $R \geq 4a$. Furthermore, F is some 2 orders of magnitude smaller than the numerical and experimental data in Figure 8b. This is because the two antiparallel chains vertically offset by a induce an $\boldsymbol{n}$ field that is nearly left−right symmetric about the line of centers for each chain. This is apparent when contrasting the insets in Figure 11a with those in Figure 8a. In the former, the dark brushes are confined within the gap between neighboring particles in the chain, while in the latter, they extend to the other particle. Thus, the antiparallel chain−chain interaction is much weaker than that between two individual particles. Such symmetry does not exist for the parallel chains in Figure 10, and thus the chain−chain repulsion is comparable to the pairwsie repulsion.

3. Multidrop Self-Assembly. We simulate the self-organization of eight droplets in a square domain of dimensions $14a \times 14a$. Periodic boundary conditions are imposed in both directions; the lack of a Dirichlet condition for $\boldsymbol{n}$ implies that the director field will evolve under the influence of the anchoring on the droplets rather than a far-field alignment. Initially, the droplets are randomly positioned in the periodic domain (Figure 12a). Similar to the preceding simulations, the initial director field is such that $\boldsymbol{n}$ is radial within a thin ribbon surrounding each droplet and uniformly vertical outside. After the simulation begins, a

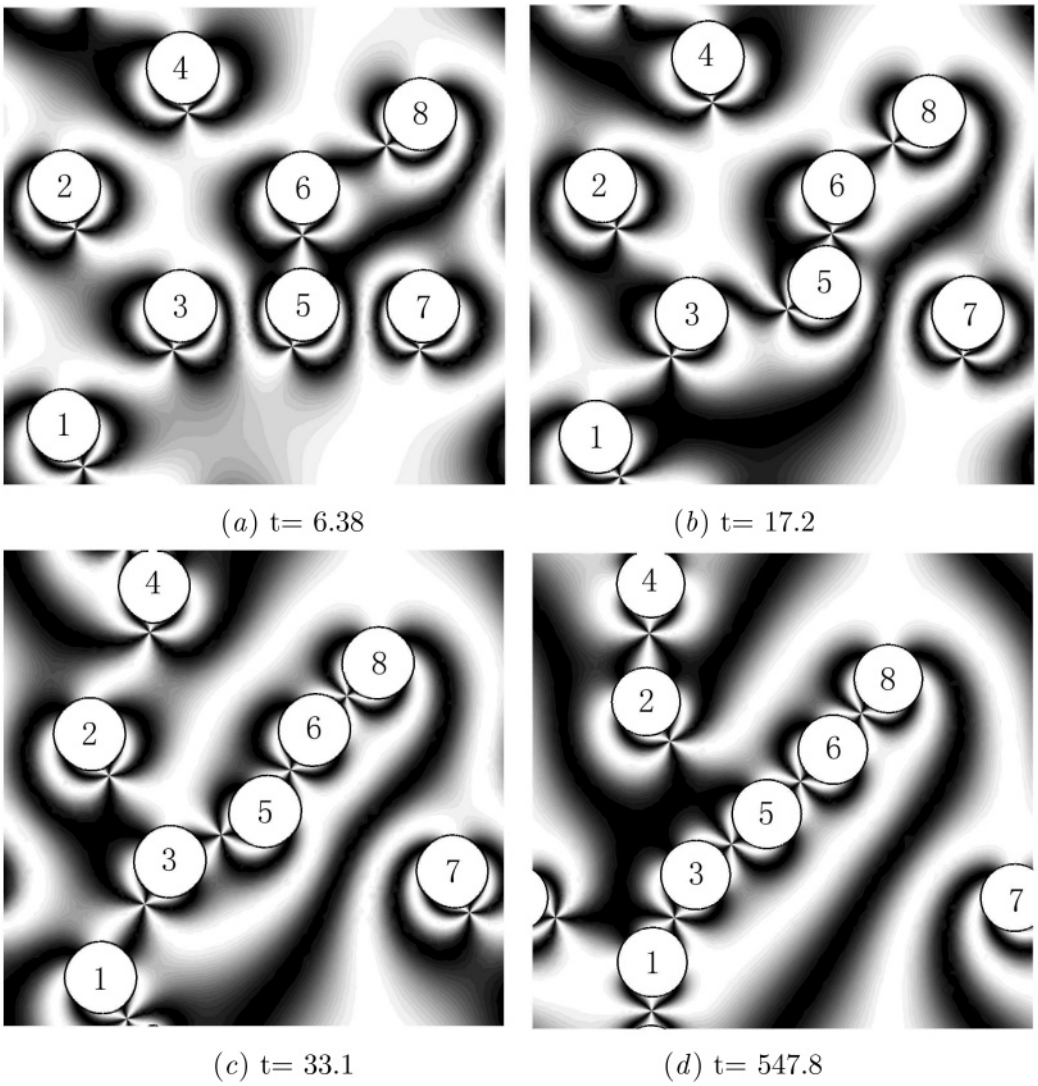

Figure 12. Self-assembly of eight drops in a doubly periodic domain. Note that the time is made dimensionless by $\eta a^2/K$.

point defect immediately nucleates near each particle (Figure 12a), which is visualized by the intersection of four dark brushes.

The ensuing self-assembly seems to be driven by the pairwise interactions discussed in Section III.A. The point defects quickly move toward the nearest neighbor so the drop−defect dipole points to the latter, similar to Figure 9. This is seen in Figure 12a for drop 8 (toward drop 6) and drop 1 (toward drop 4). This is followed, in Figure 12b, by attraction between longitudinal pairs (drops 1 and 4, 5, and 6 and 6 and 8) as well as repulsion between lateral pairs (drops 3 and 5 and 5 and 7). The repulsion between 3 and 5 is short-lived, however, as the drop-to-defect dipole for drop 5 rotates clockwise until it points toward drop 3. Afterward the two attract in a similar way to the two bottom droplets of Figure 10a. Toward the end of the simulation (t = 547.8), a predominant chain has taken shape, consisting of drops 8, 6, 5, 3, and possibly 1 (Figure 12d), oriented diagonally. Drops 1, 4, and 2 are forming a minor chain along the vertical direction. Drop 7 is the only "free" droplet at this moment but may eventually be absorbed into the diagonal chain by attraction from drops 1 and 3. Because of the double periodicity of the computational domain, the interaction among the droplets are not guided by a fixed far-field orientation, and the assembly proceeds slowly, especially in the late stage. Because of the modest number of droplets, chain−chain interaction is absent and the formation of 2D arrays cannot be simulated.

Qualitatively, the self-assembly of droplets into chains is in agreement with experimental observations in 3D nematics[3,4,9] and 2D smectic-C films.[39,42] Quantitatively, we can compare the time required for the self-assembly and the equilibrium drop spacing in the chain. Cluzeau et al.[39] reported chain formation in 2.8 s in their experiment, which translates to a dimensionless time of roughly 110. This is comparable to the timescale of chain formation in Figure 12. In the diagonal chain of Figure 12d, the point defect is more or less midway between the neighboring particles, with a distance of $1.37a$ to the drop center. Thus, the drop spacing is $R_e = 2.74a$. This is in reasonable agreement with the experimental measurements for chains both in 3D nematic ($R_e = 2.6a$)[3] and in 2D smectic-C films ($R_e = 2.6a \pm 0.2a$).[39]

The most comparable computational study seems to be that of Yamamoto and co-workers.[20,38] As mentioned in the Introduction, their scheme is quasi-static and ignores hydrodynamic effects. It amounts to assuming that the flow is much slower than elastic relaxation and thus decouples the particle motion from flow in the limit of a vanishing Ericksen number. This is perhaps justifiable in the final stage of the self-assembly, but the dynamics can be important early on as shown by our simulation of pairwise interactions. There is a second and perhaps more significant difference. The theoretical model of Yamamoto[20] is such that the satellite point defect is unstable in 2D and the pairwise interaction is of the "quadrupolar" type rather than the "dipolar" type seen

here and in most experiments. Consequently, the particles aggregate into clusters that tend to assume an angle with the far-field orientation, which is fixed in his computation. These clusters should be compared with the "kinked chains" formed of droplets bearing Saturn rings[9] or particles with planar anchoring.[6] The straight chains linked by point defects, prevalent in experiments with 3D nematics as well as 2D smectic-C films, cannot be realized using his theoretical model. In a more recent work, Yamamoto et al.[38] presented results for a smectic-C film. The free energy appears slightly different, and a stronger anchoring parameter is used. This produces satellite point defects near individual particles, which assemble into chains that are similar to ours in Figure 12. The final center-to-center separation $R_e = 2.88a$ is somewhat larger than our and previously reported experimental values. The timescale of self-assembly cannot be compared because of the quasi-static nature of their computation.

IV. Conclusion

Through dynamic simulations, we have explored the interaction of particles in a nematic medium using a more or less rigorous theory of nematohydrodynamics. The goal is to gain a more rational understanding of the self-assembly process than that has previously been achieved through analogies and ad hoc models. The results on pairwise and multiparticle interactions can be summarized as follows.

(a) The long-range attraction force between pairs of droplets, each having a point defect that is on the line-of-centers of the droplets and facing the same direction, obeys a scaling $F \sim R^{-4}$ with the drop separation R. This is the most well-established fact about pairwise interaction and is consistent with the idea of attraction between dipoles.

(b) Pairwise interaction in shorter range is poorly documented, and there is considerable discrepancy among the few theoretical and experimental studies. We have examined several configurations for the drop−defect ensemble in which the droplets attract or repel each other. The dynamic nature of the interaction is important, especially in the early stage, and the force between droplets cannot be represented by that between dipolar and quadrupolar moments.

(c) Multiple droplets form linear chains via pairwise attraction and repulsion between neighboring droplets. Preformed parallel chains repel each other if their drop-to-defect vectors are in the same direction. They attract if their orientations are reversed.

We have compared our simulations with prior static calculations and experiments to the greatest extent possible. There is qualitative, and sometimes semiquantitative, agreement. More detailed comparison is hampered by experimental complications such as the presence of substrates and difficulties in quantifying anchoring strength as well as two limitations in our simulations: two-dimensionality and the small number of particles. On a more fundamental level, a vector-based theory such as the Leslie−Ericksen model cannot describe the structure of the defect core, which may play a role in the interaction between particles in close proximity.[9] Clearly, more carefully designed experiments and sophisticated computations are needed to establish a coherent and detailed understanding of particle interaction and assembly in nematics.

Acknowledgment. Acknowledgment is made to the donors of The Petroleum Research Fund, administered by the American Chemical Society, for partial support of this research. J.J.F. was also supported by the NSERC, the Canada Research Chair program, the Canada Foundation for Innovation, and the NSFC (No. 50390095). C.Z. acknowledges partial support by a University Graduate Fellowship from UBC. We thank Siddharth Khullar for the experimental images in Figure 6 and Carl Ollivier-Gooch for help with implementing periodic boundary conditions in the code.

LA703312F